# Dynamic charge-changing processes in highly charged ions colliding with Ar atoms near the Bohr velocity

Zhao Wang [1,2] Bin Guo,[3] Rui Cheng,[1,5,6,*] Feibiao Xue,[4] Yanhong Chen,[1] Yu Lei,[1,5] Yuyu Wang,[1,5,6] Zexian Zhou,[1,2] Jie Yang,[1,5,6] Maogen Su,[2] and Chenzhong Dong[2,†]

[1]*Institute of Modern Physics, Chinese Academy of Sciences, Lanzhou 730000, People's Republic of China*
[2]*Key Laboratory of Atomic and Molecular Physics and Functional Material of Gansu Province, College of Physics and Electronic Engineering, Northwest Normal University, Lanzhou 730070, People's Republic of China*
[3]*Gansu Medical Device Inspection and Testing Institute, Lanzhou 730101, People's Republic of China*
[4]*Sichuan University, Chengdu 610000, People's Republic of China*
[5]*University of Chinese Academy of Sciences, Beijing 100049, People's Republic of China*
[6]*Advanced Energy Science and Technology Guangdong Laboratory, Huizhou 516003, People's Republic of China*

The average charge states of $^{20}$Ne$^{7+}$ and $^{131}$Xe$^{20+}$ ions penetrating through the gaseous argon targets with different areal densities are measured, and the velocities of projectile is close to the Bohr velocity regime ($v \sim 1$ a.u.). The results show that, with the increase of target density, the dynamic evolution of average charge occurs in three different stages. The dependence of the average charge state on the charge-changing cross section from the nonequilibrium stage to the equilibrium stage is revealed by the theoretical predictions that consider single-electron and additional double-electron processes. It is found that the multi-electron charge-changing process needs to be properly considered in the equilibrium stage. In addition, an analysis model is proposed to predict the average charge state of the projectile in the event of significant energy loss and to quantitatively evaluate the dependence of energy loss on the charge-changing cross section.

## I. INTRODUCTION

The charge-changing processes, one of the fundamental aspects in atomic physics, depending on the atomic numbers, shell structure and relative velocity of colliding particles, as well as the target density, are of importance [1–3].The dynamic evolution of charge states, occurring in the passage of ion-beams through targets, are determined by the properties of charge-changing collisions, which involve ion-electron and ion-atom processes, as well as photoprocesses related to radiation and absorption of photons [4]. And hence the change of projectile charge may be used to diagnose the dynamic electron (atomic) density and temperature using emission spectra in a transient process [5,6]. When an accurate estimation of charge state distribution and/or energy loss of ions after their passage through a target is needed, it is necessary to acquire the information on charge-changing cross sections caused by the collisions of interacting systems [7–12]. In principle, the charge state of ions may be widely different in plasma than that in cold matter because the dominant ion-free-electron collision induces the decrease of the electron-capture cross section and, as a result, the increase of charge state and enhanced energy loss [13–17]. The roles of charge-changing and related energy loss for ions penetrating through matter are also important for the investigation of fusion energy research [18,19]. In inertial

confinement fusion, the capsule self-burning is determined by the DT − reaction produced 3.5 MeV $\alpha$-particle stopping in the plasma surrounding; the fast particles ignition application requires a deeper understanding of charge-changing and energy loss of ions in plasma [20,21]. Furthermore, the dynamics of charge state distribution and equilibrium average charge of projectiles are of interest for mastering some new applications, such as heavy-ion tumour therapy and detection of superheavy chemical elements, as well as the development of modern intense heavy-ion accelerators which improve a new solution of warm dense matter research driven by intense heavy-ion beams in the laboratory [22–26].

The charge-changing processes for highly charged ions penetrating through gaseous targets have been discussed experimentally and theoretically in the past decades, and it is well-known that charge state distribution and average charge are strongly influenced by relevant charge-changing cross sections [3,27–31]. Explanations of the physical processes were made in terms of the atomic approach, the variation of charge composition and average charge $\bar{q}$ of the ion beam penetrating through a gaseous target can be described by the balance (rate) equations [1]:

$$\frac{d}{dx}F_q(x) = \sum_{q' \neq q} F_{q'}(x)\sigma_{q'q} - F_q(x)\sum_{q' \neq q}\sigma_{qq'}, \quad (1)$$

$$\sum_q F_q(x) = 1, \quad \bar{q} = \sum_q qF_q, \quad (2)$$

*chengrui@impcas.ac.cn
†dongcz@nwnu.edu.cn

where $x$ denotes the target areal density in $cm^{-2}$, $q$ (or $q'$) is the charge of the projectile ions after their passage through a layer with areal density $x$, $F_q(x)$ and $F_{q'}(x)$ denote the fraction of the projectile to be in a certain charge state $q$ and $q'$, respectively, and $\sigma_{ij}$ are the single- and multi-electron loss ($i < j$) and capture ($i > j$) cross sections, respectively. It should be pointed out that the balance equations (1) and (2) are only valid when the target is sufficiently dilute so that the energy loss of projectiles is negligible [1]. For few-electron projectiles and atoms, the evolution of charge fractions is governed by the single-electron charge-changing processes [4].

So far, several studies of interest have focused on the highly charged ion interaction system where there is more than one electron shell in the collision system [4]. In the case of many-electron ions in collision with neutral atoms, since the inner-shell electrons play a large and even main role, the contribution of multi-electron charge-changing cross sections to the total cross sections can reach up to 40% and more [32,33], which will strongly influence the evolution of the ion charge state. For example, for heavy ions colliding with gaseous target atoms, the contribution of multi-electron processes could be about 50%, which leads to a change by 20%–30% in the equilibrium average charge of outgoing ions [34–36]. Therefore, it is necessary and valuable to study the influence of multi-electron processes on charge state for highly charged ion collision systems.

What is more, charge-changing cross sections are strongly dependent on relative colliding velocity (kinetic energy of projectiles) [31,32]. When a gaseous target density increases sufficiently, such that the average ion energy loss becomes non-negligible, the charge-changing cross sections will change continuously with projectile velocity until projectiles exit the target, which, also in turn, influences the evolution of the average charge state. Schiwietz's [28] power law ($\bar{q} \sim v^{1+0.4/Z_p}$), where $Z_p$ is the projectile nuclear charge, can roughly describe the relevance between average charge $\bar{q}$ and velocity $v$. However, charge-changing cross sections play a bridging role between projectile velocity and charge state, for which a detailed and quantitative analysis is highly required.

In this paper, we report the experimental data on $\bar{q}$ for $^{20}Ne^{7+}$ and $^{131}Xe^{20+}$ ions in an Ar gas target with varying areal density from 0.01 to 130 $\mu g/cm^2$. The initial projectile energies were several tens of keV/nucleon, within the intermediate energy regime (0.05–500 keV/nucleon) near the Bohr velocity ($E = 25$ keV/nucleon). So far, this parameter regime features the largest theoretical uncertainties, and quantitative experimental data are lacking because both the electron capture and loss are comparable processes [13,37]. The experimental results are compared with the predictions with taking single- and double-electron loss and single-electron capture processes into account. The evidence of multi-electron effects on the dynamic evolution of average charges with target areal density is given. The theoretical description of $\bar{q}$ based on the balance equations (1) and (2) is presented too, where the electron capture and loss cross sections are predicted by using two semi-empirical scaling laws [38,39]. Moreover, the dependence of $\bar{q}$ on the projectile energy loss is discussed within the present theoretical treatment.

The system of atomic units is used throughout unless otherwise specified.

## II. EXPERIMENTAL METHOD

At the Institute of Modern Physics, Chinese Academy of Sciences (IMP CAS), an experimental setup for an ion-gaseous target was built for the low-energy regime of the Heavy Ion Research Facility in Lanzhou (HIRFL), where various ions were produced by a 18 GHz electron cyclotron resonance (ECR) ion source and accelerated to energies in keV units in the range 20 to 320 times $q$ (where $q$ is the charge state of the projectile) [14,40,41]. The available beam current ranged from 10 enA to 100 e$\mu$A. Typically, the projectile velocity was 1% of the speed of light (more or less), which was close to the Bohr velocity. Figure 1 schematically illustrates the experimental setup. As shown in Fig. 1, a pseudostatic gas target was created at the end of the accelerator section. The target gas was injected through a leak valve coupled with a gas inlet which was mounted on a flange on top of the 300-mm-long gas chamber. The pressures of the target were measured at the periphery of the target chamber using a vacuum gauge (Leybold ITR90). The vacuum system of the ion transport line was maintained by means of differential evacuation with the use of two turbo molecular pumps with an evacuation rate of 500 L/s. In this case, the length of the gas column in the target was limited by two diaphragms with 1-mm-diameter apertures. In our experiment, $^{131}Xe$ and $^{20}Ne$ ions with initial charge state 20+ and 7+ were accelerated to 5 and 1.75 MeV, respectively, and transmitted to the gaseous target regime. The outgoing ions were measured by a position-sensitive detector coupled the electrostatic parallel plates.

To obtain a high detection efficiency, a relatively high intensity of the ion beams needs to be ensured. Therefore, two X-Y deflector plates (for slight adjustment of the ion-beam transmission) and a Glaser lens (to focus the ion beam) were added to optimize the beams and their transport in the target regime. After the target, the electrostatic parallel plates with a fixed bias were used to deflect the different charged ions to arrive at different positions on the detector; as a result, the distribution of the charge state of ions was obtained. The detector consisted of two microchannel plates (MCPs), a P46 phosphor screen, and a CCD camera coupled with an optical lens. The spatial resolution was about 70 $\mu m$ and a 0.5 mm slit was placed in front of the parallel plates, which ensured sufficiently high resolution of the charge state. To measure the intensity of each charge state of ions, first the initial highly charged ions passing through the vacuum (no gas in the target chamber) were measured, where the beam current and the bias on detector were properly set to produce the signal intensity at the detector lower than its saturation value. With increasing target density, the main beam intensity decreases because the charge-changing collisions between beam ions and target atoms lead to intensity redistribution to other charge states. Therefore, within the measurement, the intensity of ions at the detector remained below saturation. To achieve a relatively small statistic error in the experiment, the ion counts were more than tens of thousands for each measurement and the total error, including the detector, beam current, ions statistic, and so on, was less than 10%.
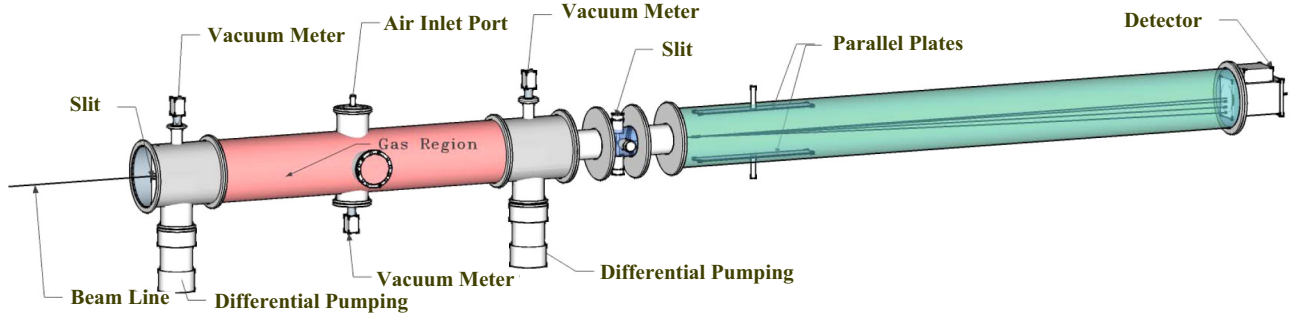
FIG. 1. Schematic illustration of the experimental setup for measuring the charge state of ions penetrating through an argon target at IMP, CAS.

## III. THEORETICAL DESCRIPTION OF THE CHARGE-CHANGING CROSS SECTIONS

Betz *et al.* outlined the basic procedures for calculation of charge-changing cross sections many years ago. As pointed out by Betz, the capture of more than one electron at a time is a relatively minor process, whereas simultaneous loss of several electrons in a single collision has a high possibility and cannot be neglected, especially for heavy ions penetrating through heavy gas targets [1]. In addition, the double-electron loss dominates the multi-electron loss process according to the experimental and theoretical data given in Refs. [32–34]. Therefore, more focus on multi-electron-loss processes (especially double-electron) is given in our discussion. In order to solve the balance equations (1) and (2), the following charge-changing cross sections are involved: single $\sigma$ (SEC) electron capture cross section and single $\sigma$ (SEL), double $\sigma$ (DEL) electron loss cross sections.

### A. Electron capture

Friedman *et al.* [38] presented the first general semi-empirical scaling law for low charged ($q < 8$) nonresonant charge-exchange collisions at intermediate velocities ($0.5 \leqslant v \leqslant 5$). In the present work, the kinetic energy of projectiles are in the range of several tens of keV/nucleon (87.5 keV/nucleon for neon ions and 38.2 keV/nucleon for xenon ions), which are close to the velocity of $v \sim 1$ (1.88 a.u. for neon ions and 1.24 a.u. for xenon ions). Correspondingly, the single-electron capture cross sections for neon ions ($q < 8$) can be calculated by using this scaling law. The cross sections can be obtained in terms of following equations:

$$
v_m = \begin{cases} 1.26\left[\dfrac{|\Delta E|}{\sqrt{q}(\sqrt{I_I}+\sqrt{I_P})}\right]^{1/2}, & q = 1, 2 \\[2em] 1.25\left[\dfrac{|\Delta E|}{\sqrt{q}(\sqrt{I_I}+\sqrt{I_P})}\right], & q > 2, \end{cases} \tag{3}
$$

$$
\begin{cases} \tilde{\sigma}_m = 6.13\exp{(-2.33\tilde{v}_m)}, & \text{with} \\ \tilde{v}_m = v_m q^{-0.89} I_T^{-0.23}, \\ \tilde{\sigma}_m = \sigma_m q^{-0.64} I_T^{1.94}, \end{cases} \tag{4}
$$

$$
\begin{cases} \tilde{\sigma}(v) = \exp\left[-\dfrac{|\tilde{v}-1|^{\tilde{m}}}{\tilde{v}^{\tilde{m}}}\right], & \text{with} \\ \tilde{v} = v/v_m, \\ \tilde{\sigma} = \sigma/\sigma_m, \\ \tilde{m} = 1.89 v_m^{0.57}, \\ \tilde{n} = 0.33 I_T^{1.09} v_m^{0.44} Z_T^{0.23} Z_p^{0.33}, \end{cases} \tag{5}
$$

where $\Delta E = I_P - I_T$ denotes the energy defect for single-electron processes, and $I_T$ and $I_P$ are the initial target and final projectile binding energies, respectively. The predictions for $I_T$, $I_P$, and $\Delta E$ use the rules described in Ref. [38] (Sec. 2.1). Using these to get $v_m$ from Eq. (3) and $\sigma_m$ from Eq. (4) can be gotten. Using both of the predictions above can get the $\sigma$ cross section in Eq. (5). The parameters $v_m$, $\sigma_m$, $q$, etc., involved in Eqs. (3)–(5), were defined in Ref. [38].

### B. Electron loss

DuBois *et al.* [39] figured out the semi-empirical scaling law of single- and multi-electron loss cross sections for any projectile colliding with argon and molecular nitrogen, which can be applied over an energy range extending from sub keV/nucleon to hundreds of MeV/nucleon. Such that we can estimate the electron-loss cross sections by the following formula:

$$
\sigma_{\text{EL}} = 11.5 v^{-1} N_{\text{p-eff}}^{0.4} [I_H/I_{\text{sum}}]^{0.59}, \tag{6}
$$

where the constant 11.5 is in units of $\pi a_0^2$, $v$ is the projectile velocity in atomic units, $N_{\text{p-eff}}$ is the effective number of projectile electrons which are available for removal. In principle, $N_{\text{p-eff}}$ is the number of outermost subshell or shell electrons of projectiles. $I_H$ is the ionization potential for atomic hydrogen, and $I_{\text{sum}}$ is the sum of the ionization potentials which is required to remove the number of electrons in a sequential manner. In our calculation, $N_{\text{p-eff}}$ and $I_{\text{sum}}$ change with different charge state; ionization potentials are obtained from the NIST database and the valuation of $N_{\text{p-eff}}$ is referred to Ref. [42] for details.

The calculated charge-changing cross sections used to solve Eqs. (1) and (2) are shown in Figs. 2(a) and 2(b) for Ne and Xe ions, respectively. SEC denotes the single-electron capture cross sections predicted using Friedman's semi-empirical scaling law [Eqs. (3)–(5)]. SEL and DEL

**(a)  Ne$^{q+}$(Z=10) +Ar  at 87.5 keV/u**
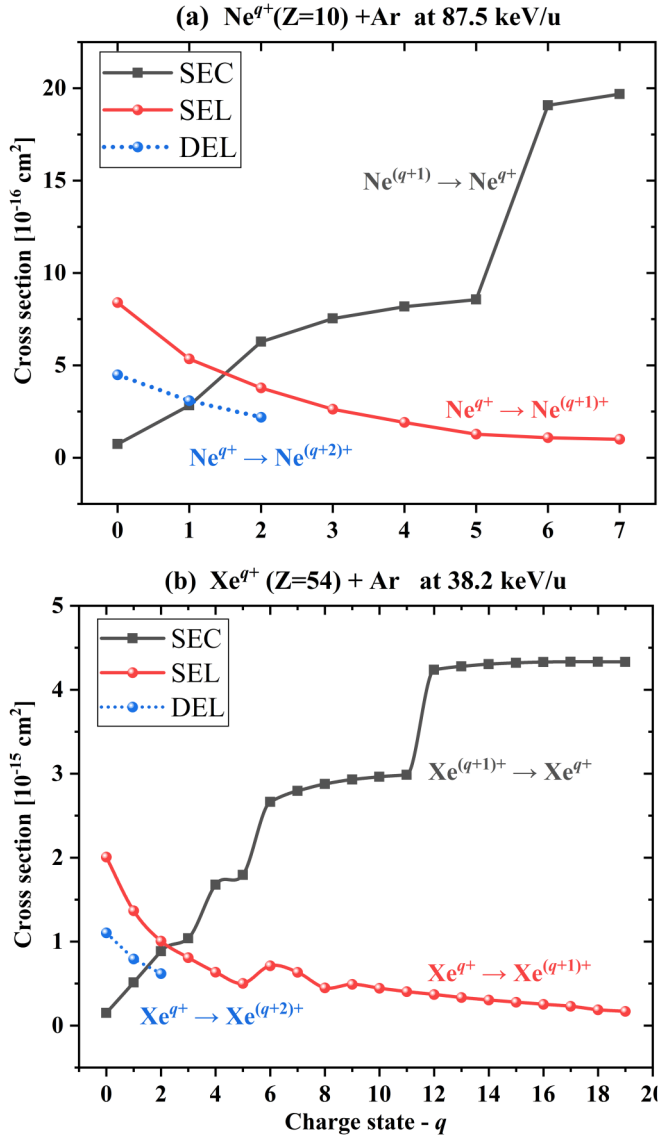


**(b)  Xe$^{q+}$ (Z=54) + Ar   at 38.2 keV/u**



FIG. 2. Electron capture (EC) and loss (EL) cross sections of $Ne^{q+}$ and $Xe^{q+}$ ions with Ar atoms at 87.5 and 38.2 keV/nucleon energy as a function of the projectile-ion charge $q$, respectively. SEC, single-electron capture cross sections, are estimated by Friedman's semi-empirical scaling law [Eqs. (3)–(5)]; SEL and DEL, single- and double-electron loss cross sections, are estimated by DuBois's scaling formula (6). The $q$ values correspond to the initial and final state of ions for the EL and EC cross sections, respectively, and the corresponding collision formulas are also shown. The lines are added to guide the eyes.

denote the single- and double-electron loss cross sections predicted using DuBois's scaling formula (6). It can be found in the figures that the $q$ value corresponds to the initial state of ions for the EL cross section while it corresponds to the final state for EC, respectively. For example, $q = 0$, the SEC corresponds to the neutralization of a singly charged ionic projectile, whereas the SEL corresponds to the creation of a singly charged projectile ion from a neutral atom.

It should be noted that all the capture cross sections of $Xe^{q+}$ ions ($0 < q \leqslant 20$) are obtained through Friedman's

**(a)  Ne$^{7+}$ (Z=10) + Ar**
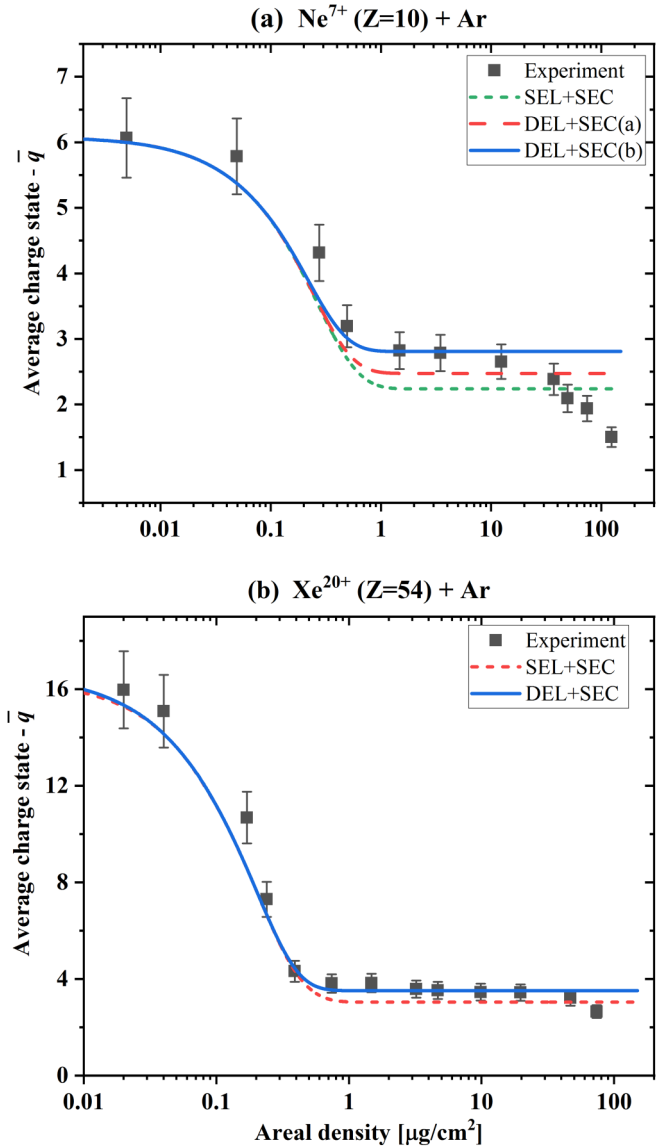


**(b)  Xe$^{20+}$ (Z=54) + Ar**



FIG. 3. Average charge states of exit ions as a function of the target areal density for (a) Ne$^{7+}$ and (b) Xe$^{20+}$ ions penetrating through gaseous Ar targets. Experimental data are shown by the square symbols. Solid, dashed, and dotted curves mark the results of the present theoretical predictions [SEL + SEC, DEL + SEC (a) and DEL + SEC (b), respectively, see text for detail].

scaling law, which claims to be appropriate for ions with low charge ($q < 8$) only (see Ref. [38]). The extended application of Friedman's scaling law for the case of $Xe^{q+}$ ions ($0 < q \leqslant 20$) colliding with argon atoms is interesting, since it is hard to find any other semi-empirical scaling laws for capture cross-section calculation for our case [38,43]. The present work can be expected to verify its applicability.

## IV. RESULTS OF THE CALCULATIONS AND COMPARISON WITH EXPERIMENT

A named BREIT code (available online [29]) was used to solve Eqs. (1) and (2). The experimental and theoretical $\bar{q}$ values for Ne and Xe ions are presented in Figs. 3(a)

and 3(b), respectively, as a function of the target areal density. In Fig. 3(a), SEL + SEC denotes the theoretical prediction with considering only single-electron loss and capture cross sections, including $\sigma_{q,q'}$ ($1 < q = q' + 1 < 7$) and $\sigma_{q'q}$ ($0 \leqslant q = q' - 1 \leqslant 6$) in Eq. (1); DEL + SEC (a) additionally, the double-electron loss cross sections $\sigma_{0,2}$ and $\sigma_{1,3}$ are taken into account; DEL + SEC (b), more than DEL + SEC (a), the cross section of $\sigma_{2,4}$ is considered. In Fig. 3(b), similarly, SEL + SEC, for single-electron loss and capture cross sections, including $\sigma_{q,q'}$ ($1 < q = q' + 1 < 20$) and $\sigma_{q'q}$ ($0 \leqslant q = q' - 1 \leqslant 19$) only; DEL + SEC is for $\sigma_{0,2}$, $\sigma_{1,3}$, and $\sigma_{2,4}$.

## A. The role of multi-electron processes on evolution of average charge states

As shown in Fig. 3(a), the experimental $\bar{q}$ value is dynamically decreasing with increasing areal density and approaching the equilibrium value of 2.78 around an areal density of about 1.48 $\mu$g/cm$^2$. Starting from 36.90 $\mu$g/cm$^2$, the $\bar{q}$ value decreases again with the areal density. Obviously, three distinguishing stages can be observed over the whole evolution of average charge, including the nonequilibrium stage ($0 < x < 1.48$ $\mu$g/cm$^2$), equilibrium stage 1 ($1.48 \leqslant x < 36.90$ $\mu$g/cm$^2$), and equilibrium stage 2 ($36.90 \leqslant x \leqslant 123.00$ $\mu$g/cm$^2$). It is important to point out that the equilibrium $\bar{q}$ and the charge distributions herein remain constant with the change of areal density only at equilibrium stage 1, corresponding to the solution of Eqs. (1) and (2) at $dF_q/dx = 0$ [4]. Apparently, the experimental data are coincident with the theoretical predictions within the error bars in the nonequilibrium stage. The effect of multi-electron charge-changing upon the average charge state seems no different compared with the single-electron process in the nonequilibrium stage. However, the difference becomes obvious in the equilibrium stages. It can be attributed to the fact that the contribution of multi-electron-loss processes increases with decreasing ion charge $q$ [2,33], since the number of active electrons from small to large and their orbital binding energy from strong to weak. More details of a comparison between the experiment and the theoretical prediction are shown in Fig. 4. As a typical case, Fig. 4(a) shows the charge state distributions and Fig. 4(b) shows the corresponding characteristic parameters, respectively, for the areal density of 1.48 $\mu$g/cm$^2$. The parameter width $d = [\sum_{q'}(q' - \bar{q})^2 F(q')]^{1/2}$ and skewness $s = \sum_{q'}(q' - \bar{q})^3 F(q')/d^3$ characterize the standard deviation and asymmetry of the distribution, respectively (see Ref. [1] for detail). Figure 4(a) shows that the equilibrium charge distribution moving to the higher charge state, while considering the double-electron loss effect, which provides better agreement with the experiment data. More clear evidence can be found in Fig. 4(b), when we take DEL + SEC (a) and DEL + SEC (b) into account, it leads to $\bar{q}$ increasing by about 10.3% and 25.4%, respectively, and makes $\bar{q}$ and $s$ approaching a much better agreement with the experimental data than the prediction of SEL + SEC only. The differences of $d$ between the experiment and all the predictions are not obvious. Thus for Ne$^{7+}$ ions with Ar atoms at equilibrium stage 1, the contribution of multi-electron-loss cannot be neglected. For the equilibrium stage 2, $\bar{q}$ goes down again and the reason can
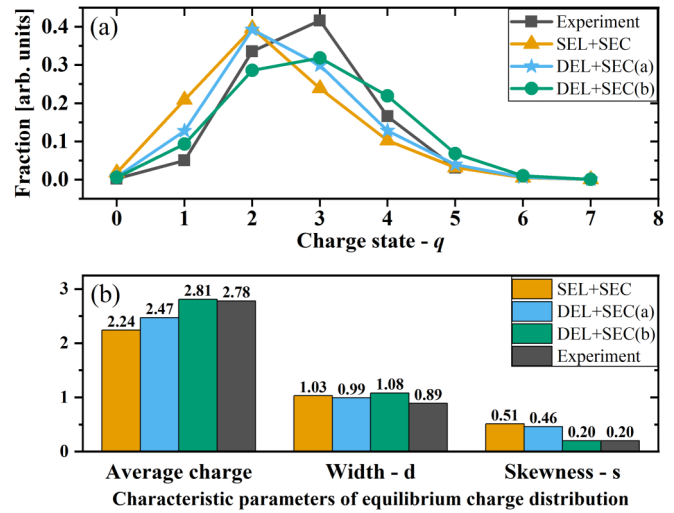


FIG. 4. (a) The typical charge state distributions at equilibrium stage 1 where the experimental data correspond to the areal density of 1.48 $\mu$g/cm$^2$, the theoretical predictions are shown, too. (b) The characteristic parameters of the equilibrium charge distributions of panel (a).

be deduced to the energy loss of projectiles, which will be discussed later.

As seen from Fig. 3(b), the change of average charge of Xe$^{q+}$ ions is similar to that of Ne$^{q+}$ ions in Fig. 3(a). However, $\bar{q}$ of Xe ions reaches equilibrium stage 2 around an areal density of 73.80 $\mu$g/cm$^2$, where the areal density is 36.90 $\mu$g/cm$^2$ for the Ne$^{q+}$ case. The experimental data for Xe ions is well reproduced by our presented theoretical predictions except for the areal density of 73.80 $\mu$g/cm$^2$. When we take the double-electron loss cross sections $\sigma_{0,2}$, $\sigma_{1,3}$, and $\sigma_{2,4}$ into account, it makes the $\bar{q}$ increase by about 15.5% and concludes a better agreement with the experiment than only considering the single-electron case. More important, this experimental evidence may be used to clarify the applicability of the Friedman's scaling law [Eqs. (3)–(5)] for the first time to be used in ion charge $q \geqslant 8$ at the intermediate-velocity regime.

## B. The influence of energy loss on average charge state

Figure 5(a) shows that the significant energy loss of the projectile (Ne ion) in the large target areal density region (equilibrium stage 2) is observed in experiment, the corresponding velocities of outgoing ions are also shown. The BREIT code, used to solve Eqs. (1) and (2), assumes the constant cross sections with respect to the areal densities and without considering energy-loss effect [29]. Obviously, that is not valid for our situation at equilibrium stage 2 where the energy loss happens.

In principle, the energy loss of a projectile ion can be obtained through the summation of the piece of energy loss that happens at every sufficiently thin layer of a target, where the ion energy and the charge-changing cross section remain constant. The ion energy in each layer is only determined by the last energy-loss process at the previous layer [29]. We propose an analysis model schematically illustrated in Fig. 5(b) in
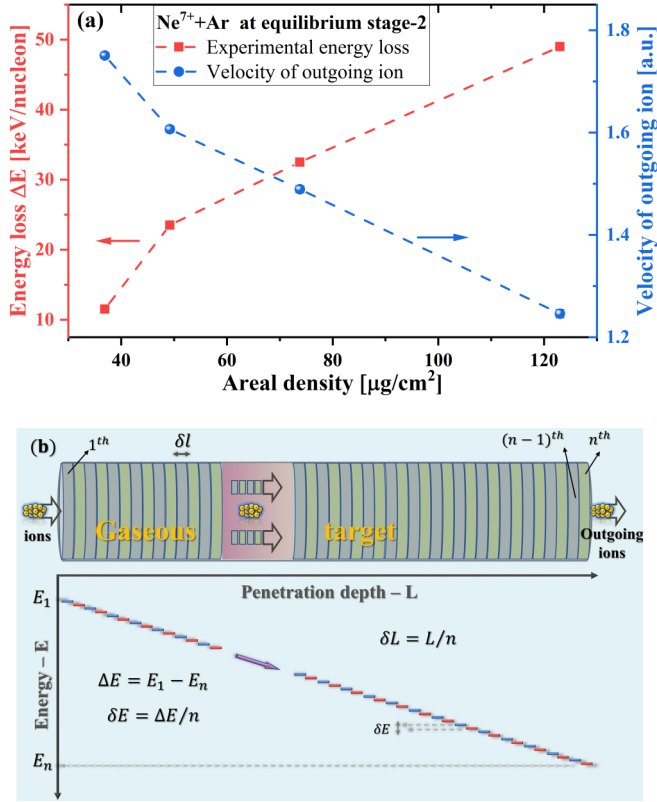
FIG. 6. The average charge states $\bar{q}$ as a function of the areal density for Ne$^{7+}$ ions penetrating through gaseous Ar targets at equilibrium stage 2. The experimental average charges shown by square symbols are taken from Fig. 3(a). The two solid lines delineate the predicted average charges, using the Schiwietz's semiempirical formula and cross-section method (SEC + SEL), respectively. The cross sections used in the cross-section method are shown in Fig. 7.

FIG. 5. (a) Experimental energy loss and corresponding velocity of outgoing ions at equilibrium stage 2 for the Ne-ion case. The error bars, smaller than the size of the symbols, are invisible. (b) The diagram of the hypotheses model we proposed to solve the average charge state of projectiles when a significant energy loss happens at equilibrium stage 2. At the top, ions are passing through the gaseous target, which is divided into $n$ sufficiently small layers. The bottom shows the evolution of the kinetic energy of ions within their penetration. Energy loss only happens at the edge between layers and the ion velocity remains constant in each layer.

order to predict the average charge state at equilibrium stage 2 by the experimental energy loss:

(i) As shown in Fig. 5(b), the penetration depth $L$ of ions in the target is divided into $n$ sufficiently thin layers $\delta l$. The total energy loss $\Delta E$ can be represented by $\Delta E = E_1 - E_n = n\delta E$, where $E_1$ and $E_n$ denote kinetic energy of ions in the first and $n$th layers, respectively; $\delta E$ is the energy loss of ions in each layer and is restricted to be sufficiently small.

(ii) Obviously, the areal densities at equilibrium stage 2 have reached the so-called equilibrium areal density (see Ref. [1]) at the present ion energy. Under the circumstances, the evolution of the ion charge state in each layer is determined only by the charge-changing cross sections but not by the initial charge state. According to Sec. III, therefore, the evolution of the charge state in each layer depends only on projectile velocity.

(iii) In the last layer, the projectile energy is approximately equal to the energy of the outgoing ions. Consequently, the projectile velocity in the last layer can be known by the experimental energy loss $\Delta E$ of outgoing ions, i.e., by Fig. 5(a). This allows us to simplify the prediction of the average charge
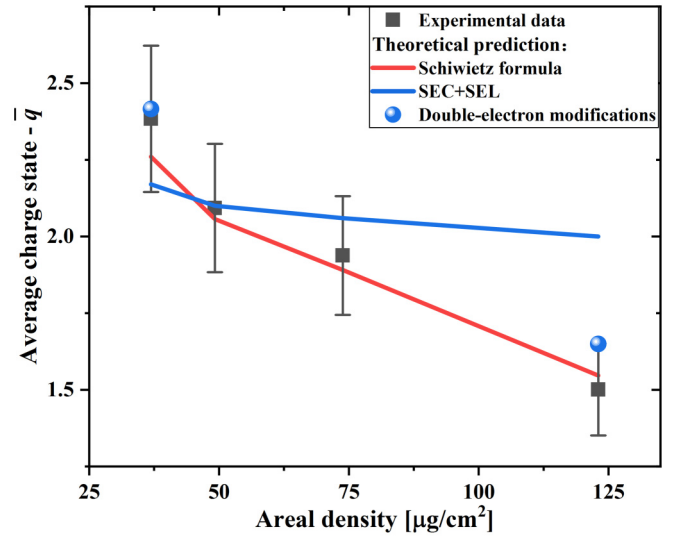
state, i.e., the average charge state of ions penetrating the whole target can be obtained merely through analyzing the ion penetration in the last layer of the target.

Then, based on the model above, the cross-section method [solve Eqs. (1) and (2) by using the BREIT code] or some empirical formula can be applied to obtain the average charge state when energy loss of projectiles happens.

Several approximate relations to estimate the average charge $\bar{q}$ in the equilibrium stage are proposed in Refs. [1,28,44,45]. Schiwietz's formula [28] in a gas and solid target providing an averaged dependence of the equilibrium average charge on ion energy without the consideration of oscillations related to the shell structures of an ion and target atom are considered the most accurate [46]. Therefore, it can be used to evaluate our model without regard to charge-changing processes. The equilibrium average charge state in a gas is given by Schiwietz's formula as follows:

$$\bar{q}_{\text{schi}} = Z_P \frac{376\xi + \xi^6}{1428 - 1206\xi^{0.5} + 690\xi + \xi^6}, \quad (7)$$

with the scaling parameter

$$\xi = [(v_P/v_0)Z_P^{-0.52}Z_T^{0.03-0.017Z_P^{-0.52}v_P/v_0}]^{1+0.4/Z_P}, \quad (8)$$

where $Z_P$ and $Z_T$ denote the nuclear charge of the ion and of the target atom, respectively. $v_0$ is the Bohr velocity, and $v_P$ is the projectile velocity. Based on our model, $v_P$ is the velocity of an outgoing ion, e.g., $v_P = 1.25$ a.u. at an areal density $x = 123.00$ $\mu$g/cm$^2$ for the Ne-ion case, according to Fig. 5(a).

Figure 6 shows the average charge states $\bar{q}$ of Ne ions as a function of target areal density at equilibrium stage 2. [The experimental data are taken from Fig. 3(a).] The theoretical
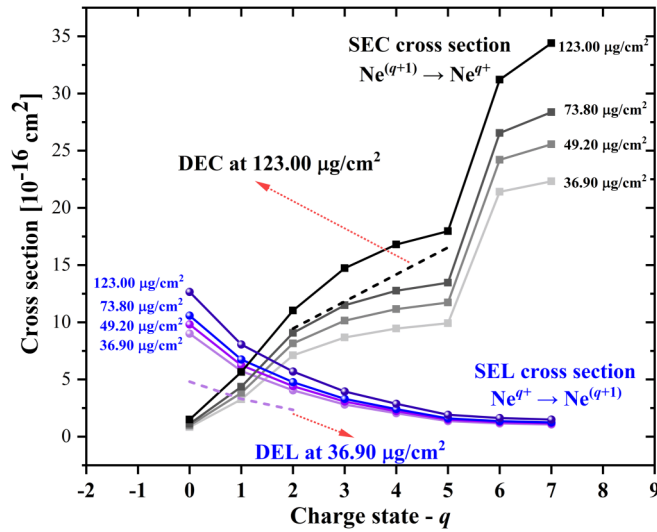
FIG. 7. Electron-capture (EC) and loss (EL) cross sections of $Ne^{q+}$ ions with Ar atoms at different areal densities as a function of the projectile ions charge $q$. SEC and DEC are single- and double-electron capture cross sections from Friedman's semi-empirical scaling law [Eqs. (3)–(5)] and the formula (9), respectively. SEL and DEL are single- and double-electron loss cross sections from DuBois's scaling formula (6). The $q$ values correspond to the initial and final state of ions for the EL and EC cross sections. The lines are added to guide the eyes.

prediction by Schiwietz's formula (red line) shows a very good agreement with the experiment, which indicates that our model is sound. Therefore, we repredict $\bar{q}$ by using the cross-section method based on our model, and the results are also shown in Fig. 6: SEC + SEL denotes the prediction only considering single-electron charge-changing cross sections. Double-electron modifications denote the prediction additionally considering double-electron cross sections. The corresponding charge-changing cross sections used to predict $\bar{q}$ by the cross-section method are shown in Fig. 7. We note that the single-electron capture and loss cross sections increase simultaneously with increasing areal density, but the rate of capture cross sections is twice as fast as the loss cross sections. As shown in Fig. 6, the differences between experiment and prediction by SEC + SEL are within the error bars, except for the areal density $x = 123.00 \, \mu g/cm^2$. The explanation for the discrepancy at this areal density (123.00 $\mu g/cm^2$) may be deduced that the multi-electron capture process becomes more important, thus a hypothetical calculation of the multi-electron capture process for our case is given.

As pointed out by Ding *et al.* [37], the cross section for pure ionization of the target is very small near the Bohr velocity energy regime ($v \sim 1$ a.u. or $E \sim 25$ keV/nucleon). Therefore, the multi-electron-capture cross sections of projectiles should be very close to the multi-electron removal cross sections of target atoms. Furthermore [37], in the velocity range of 0.65–1.32 a.u., the electron-capture cross section of highly charged ions colliding with atoms displays weak velocity dependencies. In our work, the velocity of outgoing ions is equal to 1.25 a.u. at the areal density $x = 123.00 \, \mu g/cm^2$, and thus we can predict double-electron-capture cross sections through
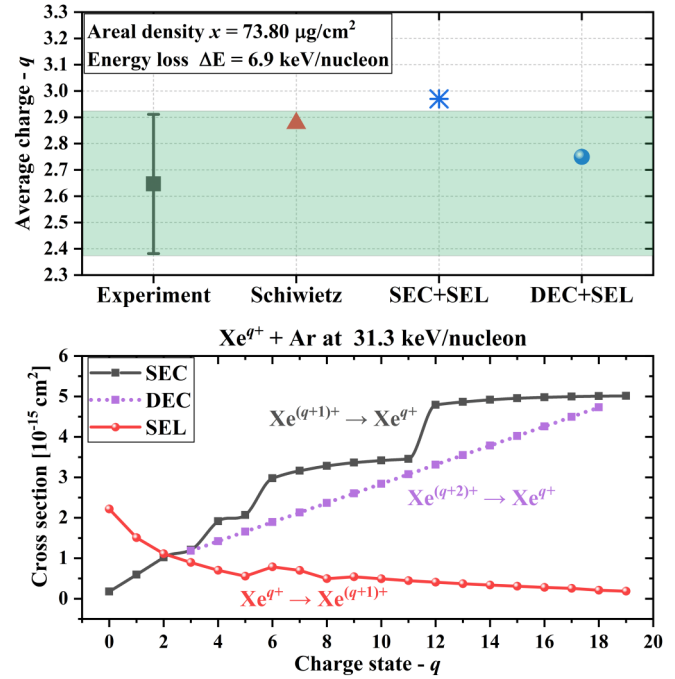


FIG. 8. (top) The comparison of average charge state between the experiment and the theoretical predictions for $Xe^{20+}$ ions penetrating through gaseous Ar target at the areal density $x = 73.80 \, \mu g/cm^2$. (bottom) Electron-capture (EC) and loss (EL) cross sections of $Xe^{q+}$ ions with Ar atoms at areal density $x = 73.80 \, \mu g/cm^2$ as a function of the ion charge state $q$. SEC and DEC are single- and double-electron-capture cross sections from Friedman's semi-empirical scaling law [Eqs. (3)–(5)] and formula (9), respectively. SEL is single-electron-loss cross sections from DuBois's formula (6). The $q$ values correspond to the initial and final state of ions for the EL and EC cross sections, respectively. The lines are added to guide the eyes.

the semi-empirical formula in which the absolute cross sections of removing $k$ electrons from the target is written as [47]

$$\sigma^k = (2.7 \times 10^{-13}) q k \left( I_k^2 \sum_{i=1}^{N} [i(I_1/I_i)^2] \right), \qquad (9)$$

where $I_i$ is the $i$th target ionization potential in eV, $N$ is the number of outer-shell electrons of the target, and $q$ is the charge state of the projectile.

In Fig. 7, the double-electron-capture cross sections predicted through formula (9) for $Ne^{q+}$ ions with Ar atoms at $x = 123.00 \, \mu g/cm^2$ are shown by dotted lines. For $x = 123.00 \, \mu g/cm^2$, incorporating double-electron-capture cross sections into the calculation, the predicted $\bar{q}$ is shown in Fig. 6 by a blue solid sphere. It is observed that the double-electron-capture effect induces a lower $\bar{q}$, which makes a better agreement with the experiment than the single-electron-capture case. So it is plausible to believe that the multi-electron capture plays a role at the areal density of 123.00 $\mu g/cm^2$. Moreover, Fig. 6 shows an additional predicted $\bar{q}$ at areal density $x = 36.90 \, \mu g/cm^2$ by considering the multi-electron effect and Fig. 7 shows the double-electron-loss cross sections. As a result, a better agreement

at $x = 36.90$ $\mu\text{g/cm}^2$ with the experiment indicates that the multi-electron-loss effect happens, too, in the small-energy-loss region.

Moving to Xe$^{q+}$ ions and argon atoms collision system which has been shown in Fig. 3(b), the change of $\bar{q}$ of Xe ions is very similar to that of Ne ions at the equilibrium stage 2. The experimental $\bar{q}$ decreases with increasing areal density too because of the increased energy loss, which has been discussed previously. At areal density $x = 73.80$ $\mu\text{g/cm}^2$ the experimental energy loss of Xe$^{q+}$ ions is equal to 6.9 keV/nucleon and the velocity of outgoing ions is equal to 1.12 a.u. This allows us to predict the double-electron-capture cross sections through formula (9). The top of Fig. 8 shows the comparison between the experiment and the theoretical $\bar{q}$ of Xe$^{q+}$ ions penetrating through the Ar target when the areal density $x = 73.80$ $\mu\text{g/cm}^2$, where the theories include Schiwietz's formula, the single-electron (SEC+SEL) and the additional double-electron (DEC+SEL) charge-changing cross sections calculations, respectively. It is found that $\bar{q}$ given by Schiwietz's formula fits the experiment within the error bar ($\sim 10\%$), which shows the evidence that our proposed model can be applied for the highly charged Xe$^{q+}$ ions at equilibrium stage 2, too. The $\bar{q}$ given by the SEC + SEL overestimates the experiment, but the $\bar{q}$ predicted by the DEC + SEL provides a better agreement with the experiment. The bottom of Fig. 8 shows the relevant charge-changing cross sections used in our theoretical calculations. Comparing with Fig. 2(b), where the projectile energy is 38.2 keV/nucleon, we note that single-electron capture and loss cross sections increase simultaneously, but the rate of capture cross section seems faster than that of the loss cross section by a factor of 1.5.

## V. CONCLUSIONS

Experimental data of the evolution of average charge states, when $^{20}$Ne$^{7+}$ and $^{131}$Xe$^{20+}$ ions penetrate through the different densities of the gaseous Ar target, are presented. The energy of Ne$^{7+}$ and Xe$^{20+}$ ions are 87.5 and 38.2 keV/nucleon, respectively. The density of Ar targets ranges from 0.01 to 123.00 $\mu\text{g/cm}^2$. The experimental results show a clear dynamic evolution of the average charge state from the nonequilibrium stage to equilibrium stage 1 and 2. In the nonequilibrium stage, the single-electron charge-changing process is dominant. In equilibrium stage 1, the multi-electron-loss process needs to be properly considered. In equilibrium stage 2, the average charge state decreases again as the projectile decelerates. This paper presents an analysis model to predict the average charge state of a projectile in the case of significant energy loss. Schiwietz's formula verifies the validity of our model. It has been figured out that the single-electron capture and loss cross sections increase simultaneously with increasing energy loss, where the rate of capture is larger by 1.5 to 2 times than that of loss. It is worth noting that this finding applies only to low energies near the Bohr velocity ($E \sim 25$ keV/nucleon). In addition, our work suggests that the contribution of the multi-electron charge-changing process should be considered in equilibrium stage 2.

Our experimental data of highly charge Xe$^{q+}$ ions show evidence that Friedman's scaling law can be used when $q \geqslant 8$ in the Bohr-velocity regime.

[1] H. D. Betz, Rev. Mod. Phys. **44**, 465 (1972).

[2] I. Y. Tolstikhina and V. P. Shevelko, Phys. Usp. **56**, 213 (2013).

[3] J. Khuyagbaatar, V. P. Shevelko, A. Borschevsky, C. E. Düllmann, I. Y. Tolstikhina, and A. Yakushev, Phys. Rev. A **88**, 042703 (2013).

[4] I. Y. Tolstikhina and V. P. Shevelko, Phys. Usp. **61**, 247 (2018).

[5] T. Schlummer, O. Marchuk, D. R. Schultz, G. Bertschinger, W. Biel, D. Reiter, and the TEXTOR-Team, J. Phys. B: At., Mol. Opt. Phys. **48**, 144033 (2015).

[6] G. Xu, M. D. Barriga-Carrasco, A. Blazevic, B. Borovkov, D. Casas, K. Cistakov, R. Gavrilin, M. Iberler, J. Jacoby, G. Loisch, R. Morales, R. Mader, S.-X. Qin, T. Rienecker, O. Rosmej, S. Savin, A. Schönlein, K. Weyrich, J. Wiechula, J. Wieser, G. Q. Xiao, and Y. T. Zhao, Phys. Rev. Lett. **119**, 204801 (2017).

[7] M. D. Barriga-Carrasco, Phys. Rev. E **88**, 043107 (2013).

[8] A. Frank, A. Blažević, V. Bagnoud, M. M. Basko, M. Borner, W. Cayzac, D. Kraus, T. Hessling, D. H. H. Hoffmann, A. Ortner *et al.*, Phys. Rev. Lett. **110**, 115001 (2013).

[9] A. Ortner, A. Frank, A. Blažević, and M. Roth, Phys. Rev. E **91**, 023104 (2015).

[10] P. Sigmund and A. Schinner, Nucl. Instrum. Methods Phys. Res., Sect. B **382**, 15 (2016).

[11] R. A. Wilhelm, E. Gruber, V. Smejkal, S. Facsko, and F. Aumayr, Phys. Rev. A **93**, 052708 (2016).

[12] R. A. Wilhelm and P. L. Grande, Commun. Phys. **2**, 89 (2019).

[13] W. Cayzac, A. Frank, A. Ortner *et al.*, Nat. Commun. **8**, 15693 (2017).

[14] Y. T. Zhao, Y. N. Zhang, R. Cheng, B. He, C. L. Liu, X. M. Zhou, Y. Lei, Y. Y. Wang, J. R. Ren, X. Wang *et al.*, Phys. Rev. Lett. **126**, 115001 (2021).

[15] K.-G. Dietrich, D. H. H. Hoffmann, E. Boggasch, J. Jacoby, H. Wahl, M. Elfers, C. R. Haas, V. P. Dubenkov, and A. A. Golubev, Phys. Rev. Lett. **69**, 3623 (1992).

[16] T. Peter and J. Meyer-ter-Vehn, Phys. Rev. A **43**, 2015 (1991).

[17] I. Y. Tolstikhina, S. N. Andreev, L. A. Vainshtein, and V. P. Shevelko, J. Quant. Spectrosc. Radiat. Transfer **246**, 106944 (2020).

[18] S. Kawata, T. Karino, and A. I. Ogoyski, Matter Radiat. Extrem. **1**, 89 (2016).

[19] R. Janev, M. Harrison, and H. Drawin, Nucl. Fusion **29**, 109 (1989).

[20] O. A. Hurricane, D. A. Callahan, D. T. Casey *et al.*, Nat. Phys. **12**, 800 (2016).

[21] M. Roth, T. E. Cowan, M. H. Key, S. P. Hatchett, C. Brown, W. Fountain, J. Johnson, D. M. Pennington, R. A. Snavely, S. C. Wilks *et al.*, Phys. Rev. Lett. **86**, 436 (2001).

[22] D. Schardt, T. Elsässer, and D. Schulz-Ertner, Rev. Mod. Phys. **82**, 383 (2010).

[23] A. Nikoghosyan, D. Schulz-Ertner, B. Didinger *et al.*, Int. J. Radiat. Oncol. Biol. Phys. **58**, 89 (2004).

[24] C. E. Düllmann, R.-D. Herzberg, W. Nazarewicz, and Y. Oganessian, Nucl. Phys. A **944**, 1 (2015).

[25] R. Cheng, Y. Lei, X. Zhou *et al.*, Matter Radiat. Extrem. **3**, 85 (2018).

[26] J. Braenzel, M. D. Barriga-Carrasco, R. Morales, and M. Schnürer, Phys. Rev. Lett. **120**, 184801 (2018).

[27] S. Datz, H. O. Lutz, L. B. Bridwell *et al.*, Phys. Rev. A **2**, 430 (1970).

[28] G. Schiwietz and P. L. Grande, Nucl. Instrum. Methods Phys. Res., Sect. B **175-177**, 125 (2001).

[29] N. Winckler, A. Rybalchenko, V. P. Shevelko *et al.*, Nucl. Instrum. Methods Phys. Res., Sect. B **392**, 67 (2017).

[30] H. H. Loand and W. L. Tite, At. Data Nucl. Data Tables **1**, 305 (1969).

[31] Z. Wang, R. Cheng, F. B. Xue *et al.*, Phys. Scr. **95**, 105404 (2020).

[32] A. N. Perumal, V. Horvat, R. L. Watson *et al.*, Nucl. Instrum. Methods Phys. Res., Sect. B **227**, 251 (2005).

[33] R. L. Watson, Y. Peng, V. Horvat, G. J. Kim, and R. E. Olson, Phys. Rev. A **67**, 022706 (2003).

[34] V. P. Shevelko, N. Winckler, and M. S. Litsarev, Nucl. Instrum. Methods Phys. Res., Sect. B **330**, 82 (2014).

[35] V. P. Shevelko, I. L. Beigman, M. S. Litsarev *et al.*, Nucl. Instrum. Methods Phys. Res., Sect. B **269**, 1455 (2011).

[36] I. Y. Tolstikhina, M. S. Litsarev, D. Kato *et al.*, J. Phys. B: At., Mol. Opt. Phys. **47**, 035206 (2014).

[37] B. Ding, D. Yu, F. Ruan, R. Lu, C. Shao, C. Wan, S. Chen, and X. Cai, Phys. Rev. A **82**, 032703 (2010).

[38] B. Friedman and G. DuCharme, J. Phys. B: At., Mol. Opt. Phys. **50**, 115202 (2017).

[39] R. D. DuBois, A. C. F. Santos, and R. E. Olson, Nucl. Instrum. Methods Phys. Res., Sect. A **544**, 497 (2005).

[40] R. Cheng, Y. Zhao, X. Zhou *et al.*, Phys. Scr. **T156**, 014074 (2013).

[41] Y. Zhao, Z. Hu, R. Cheng *et al.*, Laser Part. Beams **30**, 679 (2012).

[42] A. C. F. Santos and R. D. DuBois, Phys. Rev. A **69**, 042709 (2004).

[43] H. Knudsen, H. K. Haugen, and P. Hvelplund, Phys. Rev. A **23**, 597 (1981).

[44] V. S. Nikolaev and I. S. Dmitriev, Phys. Lett. A **28**, 277 (1968).

[45] K. Shima, T. Ishihara, T. Miyoshi, and T. Mikumo, Phys. Rev. A **28**, 2162 (1983).

[46] N. V. Novikov and Y. A. Teplova, J. Surf. Invest.: X-Ray, Synchrotron Neutron Tech. **8**, 206 (2014).

[47] N. Selberg, C. Biedermann, and H. Cederquist, Phys. Rev. A **54**, 4127 (1996).